Erschienen in: Advanced Functional Materials ; 21 (2011), 5. - S. 879-890
https://dx.doi.org/10.1002/adfm.201000849

Impact of Metal Contamination in Silicon Solar Cells

Gianluca Coletti, Paula C. P. Bronsveld, Giso Hahn, Wilhelm Warta, Daniel Macdonald, Bruno Ceccaroli, Karsten Wambach, Nam Le Quang, and Juan M. Fernandez*

The impact of the transition metals iron, chromium, nickel, titanium and copper on solar-cell performance is investigated. Each impurity is intentionally added to the silicon feedstock used to grow p-type, directionally solidified, multicrystalline silicon ingots. A state-of-the-art screen-print solar-cell process is applied to this material. Impurities like iron, chromium and titanium cause a reduction in the diffusion length. Nickel does not reduce the diffusion length significantly, but strongly affects the emitter recombination, reducing the solar-cell performance significantly. Copper has the peculiarity of impacting both base-bulk recombination as well as emitter recombination. Two models based on the Scheil distribution of impurities are derived to fit the degradation along the ingot. Solar-cell performances are modelled as a function of base-bulk recombination and emitter-bulk recombination. The model fits the experimental data very well and is also successfully validated. Unexpectedly, the distribution of impurities along the ingot, due to segregation phenomena (Scheil distribution), leaves its finger-print even at the end of the solar-cell process. A measure of impurity impact is defined as the level of impurity that causes a degradation in cell performance of less than 2% up to 90% of the ingot height. The advantage of this impurity-impact metric is that it comprises the different impurities' physical characters in one single parameter, which is easy to compare.

1. Introduction

Solar-energy conversion to electricity is growing rapidly. More than 80% of the global solar-cell production is based on silicon.[1] The availability of silicon of sufficient perceived chemical purity (>7 N) has been probably the most-important bottleneck for further growth during specific time periods. The excessive cost of investment for conventional poly-Si production plants is a barrier to solving this bottleneck, a barrier which tends to become more relevant during periods of financial crisis. Furthermore, there will be greater consideration given to technologies with reduced energy-payback times and with lower carbon footprints. Therefore, there is a strong need for low-cost and low-investment-cost technologies for the production of silicon for solar cells. However, such low-cost-production technologies will most likely compromise the purity of the resultant silicon. For example, construction materials (e.g., steel or graphite used in new types of reactors) or reactants (e.g., Zn to reduce chlorosilane, C, Al) may influence the quality of the silicon. Also, some low-cost-production technologies rely on not purifying the raw (metallurgical) silicon to the same extent as conventional technologies. Therefore, it is crucial to have accurate specifications for concentrations of impurities that could be allowed in silicon feedstock for solar cells (commonly described as ' solar-grade silicon') without risking the ambitious yield and cost targets on the system level and achieving shorter energy-payback times at the same time.

Groundbreaking research performed in the 1970s and 1980s by Westinghouse Corp[2] (WH study) is still used as a reference for the effect of impurities on solar-cell performance. However, because of numerous improvements in cell processes since

G. Coletti, P. C. P. Bronsveld
ECN Solar Energy
Westerduinweg 3, Petten, NL-1755 LE, The Netherlands
E-mail: coletti@ecn.nl
Prof. G. Hahn
University of Konstanz
Department of Physics
Konstanz, 78457, Germany
Dr. W. Warta
Fraunhofer Institute for Solar Energy Systems (ISE)
Heidenhofstr. 2, Freiburg, 79110, Germany
Dr. D. Macdonald
School of Engineering
College of Engineering and Computer Science
Australian National University
Canberra, ACT 0200, Australia
Dr. B. Ceccaroli
now at: Marche AS, P.O. Box 8309
Vaagsbygd Kristiansand, NO-4622, Norway
Dr. K. Wambach
Sunicon AG, Alfred-Lange-Str. 15, Freiberg, D-09599, Germany
Dr. N. Le Quang
PhotoWatt International S. A., 33, Rue Saint-Honore-Z.L. Champfleuri
Bourgoin-Jallieu, 38300, France
Dr. J. M. Fernandez
BP Solar España, P. E. Arroyo de la Vega
Avda. de Bruselas 36, Alcobendas, 28108, Spain

then, and the increased use of directionally solidified, multicrystalline ingots[3] instead of single-crystalline ingots, there is a need for updated and more-detailed studies.

In this work we study the impact of iron, chromium, nickel, titanium and copper on p-type, multicrystalline silicon (mc-Si) ingots, with particular emphasis on the properties of the solar cells and the detrimental effect on the solar-cell performance.

Iron is a dominant metal impurity in silicon, and, being a relatively fast-diffusing impurity, is sensitive to gettering. Chromium and nickel, as components of steel together with iron, are widely employed as construction materials for equipment, often resulting in significant silicon contamination. Copper is a fast-diffusing impurity, having a high mobility even at room temperature: therefore contamination and in-diffusion of copper is not unlikely. In addition Cu is used as a catalyst in the production of fluidized-bed-reactor polysilicon. Titanium is a slow diffuser and easily forms oxides at high temperature: therefore its in-diffusion is unlikely. However, if present in the molten silicon (e.g., from the polysilicon, crucible, silicon nitride coating, etc.) it can be incorporated in the silicon ingots, from where it cannot precipitate or be gettered, and therefore is very detrimental to the minority-charge-carrier lifetime. Essentially, these impurities exhibit a wide range of physical properties (e.g., diffusivity, solubility, segregation coefficient, etc.). Therefore the extent of precipitation and gettering are expected to be significantly different, and this group of metals can be considered as model impurities for the behavior of other impurities with similar characteristics.

It is important to note that, in this study, the impurities are introduced in the silicon charge and are, of course, subject to a similar thermal history and process, as would any impurity be in the feedstock. The thermal history of the material determines, among other aspects, the fraction of impurities that are electrically active in the Si and the properties of precipitates, for example, and thus the final impact of impurities on the solar-cell performance. Therefore, the behavior of impurities in our study, including interactions of impurities with extended defects like dislocations, grain boundaries or precipitates, is as close as possible to the behavior of impurities during the entire solar-cell manufacturing value-chain. Our experimental approach differs from several previous studies (e.g., ref.[4]) where impurities were introduced by ion implantation or intentional surface contamination at the wafer level, followed by thermal annealing of the wafer.

In this article, we discuss the impact on the solar-cell performance, while a separate article describes the segregation coefficients of the impurities and the interaction between the impurities and the crystallization process, causing an increased concentration of extended-crystal defects[5] (e.g., grain boundaries and highly dislocated areas). We believe our studies are representative and useful for the assessment of the impact of unwanted impurities in feedstock and crystallization materials (e.g., crucible, Si_3N_4 coating, construction materials, etc.).

2. Background

2.1. Comparisons of the Westinghouse Model/Study with this Model/Study

In the 1970s, a thorough investigation on the impact of impurities was carried out as part of the Low-Cost Solar Array (LCSA) project, a.k.a. the "Westinghouse study". This investigation, carried out on Czochralski (Cz) ingots, examined a very wide range of impurities. The main differences between the LCSA investigation and the investigation carried out in this project are listed in **Table 1**.

Among the most important of these differences are that the data reported here refer to a modern, state-of-the-art, industrial screen-print solar-cell process,[7] that the impact of impurities is investigated on directionally solidified, multicrystalline material, as opposed to Czochralski silicon ingots. In this work, the direct relationship between impurities in the feedstock and the final solar-cell performance is reported and analyzed. This provides the most-straightforward and meaningful interpretation, especially addressed at specifying feedstock impurity tolerances. Our conclusions, therefore, do not rely on impurity analysis or estimated segregation coefficients. By comparison, the previous

Table 1. Main differences between the studies performed in the Low-Cost Solar Array (LCSA) project and in the CrystalClear (CC) project.

	LCSA	CC
Crystallization	Cz (mainly mono, some multi)	Bridgman (directional solidification)
Resistivity p-type	3.5 Ω cm	1.2 Ω cm
Cell thickness	275 µm	185 µm
Cell structure	No ARC,[a] no back surface field (BSF)	SiN_x, Al-BSF
Area	1 cm^2	156 cm^2
Average efficiency reference ingot	9.5% (14.1% with ARC) on mono	15.5% on multi
Fabrication/optimization	No optimization, high reproducibility	No optimization, high reproducibility
Cell process	Lab state of the art ~1978	Industry state of the art ~2008
Device model	Analytical solution of transport equations for a single wavelength	Numerical solution of the transport equations PC1D[6]
Data	Efficiency versus wafer impurity concentration, k_{eff} determined by NAA[a] and SSMS[a]	Efficiency versus added impurity concentration; no intermediate parameter

[a] Anti Reflection Coating (ARC), Neutron Activation Analysis (NAA), Spark Source Mass Spectroscopy (SSMS)

Westinghouse studies reported the impurity concentrations in the wafers, determined by the effective segregation coefficients, versus the solar-cell performance.

In addition, in this study the total ingot height, which corresponds to 100% of the melt weight, was used for the evaluation, as opposite to one section analyzed in the LCSA project. Therefore, each ingot provides a broad range of impurity-concentration levels of interest.

The model used here takes into consideration the distribution of impurities along the ingot height. To extract the model parameters, the entire set of data along the ingot height was used. This was necessary because it was of great importance to relate the impact of impurities to the usable fraction of the ingot in order to gain insight into the contamination level allowed.

3. Method

The concentration of impurities in commercially available silicon wafers is usually too low to be detected using commonly available techniques, and unintentional contamination during sample preparation increases the possibility of measurement artifacts. In addition, it is quite difficult to obtain material with a significant variation of one specific impurity alone, or a specific combination of impurities, with the aim of identifying their impact. For these reasons, we intentionally contaminated silicon feedstock with known amounts of single impurities as described in **Table 2**.

Impurities change their state and concentration during the manufacturing of solar cells. The processes that mainly affect the impurities are (in processing sequence): crystallization, emitter formation, SiN_x:H deposition, and metal-contact formation. During these processes, phenomena like impurity segregation, internal and external gettering, and bulk defect passivation change the concentration and the recombination activity of such impurities. The approach used in this work has the advantage of revealing the impurity impact along the entire production chain.

Table 2. Ingot descriptions: the boron and the impurity were introduced in the silicon charge, with the exception of titanium, which was added after complete silicon melting.

Element added	Label[a)]	Boron [ppm wt (ppma)]	Concentration added [ppm wt (ppma)]
–	Ref (2x)	0.13 (0.34)	Reference
Fe	Fe 50	0.13 (0.34)	53 (27)
	Fe 200	0.13 (0.34)	200 (101)
Cr	Cr 4	0.13 (0.34)	4.08 (2.20)
	Cr 40	0.13 (0.34)	40.4 (21.8)
	Cr 200	0.13 (0.34)	200 (108)
Ni	Ni 40	0.13 (0.34)	36.7 (17.6)
	Ni 200	0.13 (0.34)	203 (97.1)
Ti	Ti 10	0.13 (0.34)	9.3 (5.5)
Cu	Cu 100	0.13 (0.34)	97 (43)

[a)] Results for Fe 50 were reported by Coletti et al.[15]

The amounts of impurities added were chosen such that they targeted typical levels of impurities in commercially produced, directionally solidified, multicrystalline silicon wafers,[8–9] while aiming for a noticeable effect on both the wafer and cell levels in comparison with an uncontaminated reference material. An equilibrium segregation coefficient for this selection was assumed.[2]

The prepared contaminated feedstock was used to produce ingots in a small-scale Bridgman type Crystalox DS 250 furnace. This furnace allowed the growth of 12 kg ingots by the directional-solidification method, with a diameter of 250 mm and a height of 110 mm. The ingots were grown at Sintef in Norway. Almost all of the impurities studied were introduced together with the feedstock before the melting took place. Titanium was the only exception, due to its affinity to react with oxygen and form a wide range of oxides. In order to reduce their formation, titanium was added to the melt after complete melting had been detected.

Together with the chosen metal impurity, boron was added, targetting a base p-type doping level of about 1 Ω cm (see Table 2).

In order to minimize and, even more importantly, to control any unintentional contamination, the following precautions were adopted for the ingot solidification: i) prime quality polysilicon feedstock; ii) electronic-grade crucible[10] made of fused quartz; iii) purified silicon nitride coating as described in ref.[11]

The unintentional contamination of each ingot, though minimal, can be considered to be approximately the same. Two reference ingots without any addition of impurities were grown in the same conditions. The reference ingots gave an average, as-grown minority-carrier lifetime of about 60 μs in the middle of the ingot. This level is typical for high-quality, commercial, multicrystalline material. In this condition, the added impurity acts like a perturbation (in most cases large) of the "normal" contamination levels. This allows them to be studied in combination with a background level of impurities without a significant interaction.

Impurities can interact with each other[12] reducing their overall impact. In this way their impact is no longer simply a linear combination of the single impurities. In this paper, we study the impact of single impurities and we leave the impact of impurity combinations to a future publication.

The levels of interstitial oxygen and substitutional carbon in the as-grown wafers were approximately 8 ± 2 ppma and 2 ± 2 ppma, respectively, as measured by FTIR spectroscopy,[13] which is in the concentration range of typical, commercial, multicrystalline ingots.

A selection of 200 μm-thick wafers, from about 10 positions from the bottom to the top of the ingots, was subjected to the p-type solar-cell process. The solar-cell process is a state-of-the-art industrial process including P-diffusion, Al-Back Surface Field (BSF) SiN_x:H firing through.[7]

The same process was applied to the contaminated material, as well as to the reference material. No process optimization was carried out for the contaminated ingots since, for this investigation, we were studying the impact of the impurities on a stable, reference cell process. For this reason, this investigation

might be more restrictive in terms of allowed impurity levels. Indeed the contaminated ingots might benefit from improved processing (e.g., optimized gettering either external or internal and optimized hydrogenation)[14] depending on the impurity species present.

Throughout this paper, we use the notation "Xx *YY*" to identify the different ingots, where Xx represents the element and *YY* the amount added to the feedstock. For example, Cr 40 refers to the multicrystalline silicon ingot intentionally contaminated with 40 ppm wt of chromium.

Results of the ingot with 50 ppm wt of iron were reported by Coletti et al.;[15] however, for completeness and comparison, some results from this ingot are also reported in this paper.

4. Results and Discussion

4.1. Impact on the Solar-Cell Efficiency

In **Figure 1**, the efficiencies of the solar cells produced from wafers of the contaminated ingots are shown as a function of the ingot height. For all of the contaminated ingots, the solar-cell performances were best and, in some cases comparable to the reference, uncontaminated solar cells, in the range of 40–70% of the ingot height. Roughly, the efficiency results of the contaminated ingots can be divided into 3 regions: a bottom region up to 40% where the efficiency was lowered, a middle region from about 40 to 70% where the performance was best, and a top region above 70% of the ingot height where again the efficiency decreased towards the top.

The efficiency reduction in the bottom and on the side of directionally solidified, multicrystalline ingots is a known effect[16] due to the contact of the ingot with the crucible and the Si_3N_4 coating. The efficiency reduction observed in the bottom of the contaminated ingots was more extended than in the reference ingot (below 10% of the ingot height). The cause for this extended degradation near the bottom cannot be related to the in-diffusion of impurities from the crucible or coating, since approximately the same conditions (e.g., melting time, crystallization time and cooling) were applied for the casting of all the ingots. Indeed a poorer crystallographic structure has been reported[15] in the Fe 50 ingot, in comparison with the reference ingot. Smaller grains and highly dislocated areas were found in the bottom and top of the ingot. In this study, we found that the degradation in the bottom increased with the impurity level in the feedstock (see Figure 1). In addition to iron, this degradation was visible for chromium, nickel and copper. In the case of titanium, the efficiency degradation was so large that it was difficult to discriminate a possible bottom effect from the segregation effect. However, this does not always correspond to an increase in the crystallographic defect density.[17]

The performance degradation in the top of the ingot is a well-known effect as well. During crystallization, impurities segregate into the molten phase. Most transition metals have such a small segregation coefficient that we can consider the amount of impurities actually depleted from the molten-silicon interface to be negligible. At the same time, the molten volume decreases as the crystallization proceeds. At 90% of the growth, the molten volume is 10 times smaller, which means, due to the negligible depletion, that a 10-times-higher concentration of impurities is in the melt, and therefore in the solid as well, in comparison to the initial concentration. At 99% of the growth the concentration is 100 times higher and so forth.

In addition, immediately after crystallization completion and during the cooling the impurities diffuse back from the top, spreading their concentration. This phenomenon is limited by the cooling rate and impurity diffusivity to a small fraction of the ingot height.

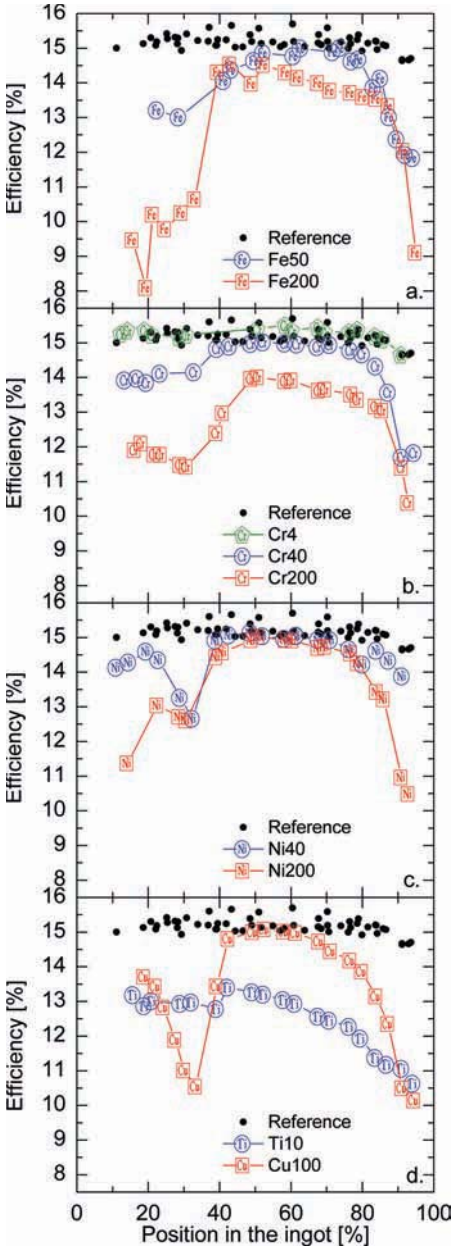

Figure 1. Solar-cell efficiency versus position along the ingot height from the bottom: a) Ingots contaminated with 50 and 200 ppm wt of iron; b) Ingots contaminated with 4, 40 and 200 ppm wt of chromium; c) Ingots contaminated with 40 and 200 ppm wt of nickel; d) Ingots contaminated with 10 ppm wt of titanium and 100 ppm wt of copper.

The efficiency reduction observed in the top of the contaminated ingot can therefore be explained by the combination of these effects. If the degradation in the reference ingot is visible at 99% of the ingot height, an ingot with a 10-times-higher impurity concentration shows this degradation at 90% and so forth. In the next section, we describe a model based on the segregation of impurities to verify that, indeed, segregation is the leading mechanism that explains the degradation trend towards the top of the ingots.

4.2. Impact on the Internal Quantum Efficiency

In order to understand the degradation mechanisms observed and their causes, the internal quantum efficiency (IQE) of the solar cells was calculated from the spectral response and reflectance measurements (see **Figure 2** as an example for the ingot with Ti 10). In **Figure 3**, the relative IQEs at 400 nm and 1000 nm compared to the reference ingot at the respective wavelength are shown for each contaminated ingot as a function of the ingot position from the bottom to the top. We chose to report the IQEs only at these wavelengths for clarity of the figures.

The IQE at 400 nm gives information on the emitter recombination due to the shallow absorption of these photons in silicon. Below 400 nm, the absorption in the SiN_x antireflecting layer needs to be taken into consideration, complicating the analysis unnecessarily.

On the other hand, photons with a wavelength of 1000 nm are absorbed deep in the silicon wafers. Therefore, IQEs at this wavelength are linked to the minority-carrier diffusion length, as well as to the rear surface conditions, in terms of both passivation and reflection. Since a highly reproducible solar-cell process was applied and assuming that the properties of the rear surface were not changed by the presence of impurities, the IQEs variation at 1000 nm was directly linked to variations in the base-bulk recombination. On the other hand, if the impurities do interact with the rear surface (e.g., degrading the surface passivation) the IQE at 1000 nm will be reduced, resulting in an overestimation of the base-bulk recombination. However, such an interaction is unlikely, and so we interpreted the IQE at 1000 nm to be related only to base-bulk recombination.

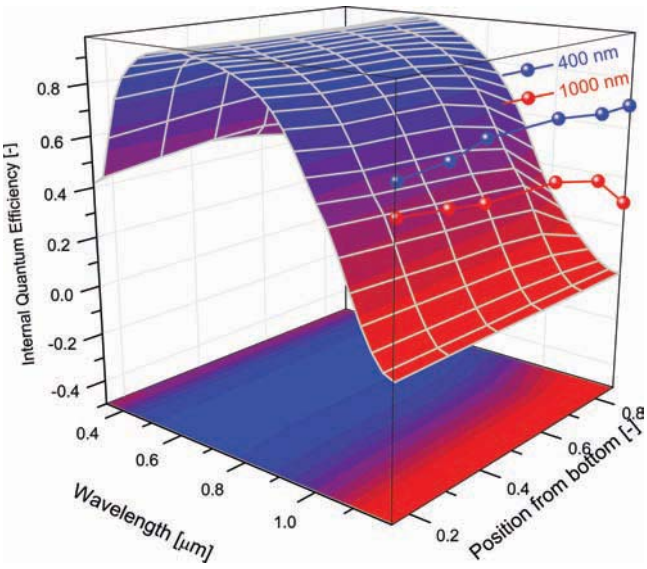

Figure 2. IQE versus wavelength and position in the ingot for the ingot with 10 ppm wt of titanium. The IQE at long wavelength (e.g., 1000 nm) decreases towards the top of the ingot. The inset shows the IQEs at 400 nm and 1000 nm, which are related to the emitter recombination and the base recombination, respectively.

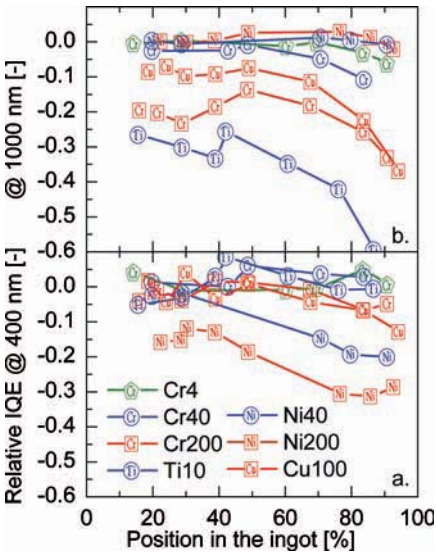

Figure 3. Relative IQE versus position in the ingot from the bottom, at a wavelength of 400 nm (a) and 1000 nm (b). The IQE at 400 nm represents the recombination in the emitter region while the IQE at 1000 nm represents the recombination in the bulk. Chromium, iron (not shown) and titanium reduce the IQE at long wavelength (1000 nm). Nickel reduces the IQE at short wavelength (400 nm). Copper reduces the IQE at both long and short wavelengths.

Iron, chromium and titanium led to an increase in the base-bulk recombination. The base-bulk recombination scaled with the impurity level as expected. In addition it increased with the ingot height as expected, considering the segregation of impurities into the liquid phase during the crystallization. The ingot with 50 ppm wt of iron showed such an increase also in the bottom, while in the ingot with 200 ppm wt, this effect was present but masked by the lower IQE at 1000 nm along the overall ingot.

These impurities did not lead to any increase of emitter recombination along the overall ingot. This suggests that, even in the very top of the ingots, the high concentrations of Fe, Cr, and Ti did not affect the emitter recombination, at least to the levels that the solar-cell performances were reduced. Despite the fact that gettering to the emitter was very effective, for example, for Fe and Cr, as evident from the negligible impact of such impurities in the middle of the ingot, the accumulation of atoms in the emitter region did not cause additional noticeable recombination.

Nickel did not show an increase in the base-bulk recombination. Even the highest concentration introduced in the feedstock (200 ppm wt) did not cause a visible effect at long wavelengths. Therefore, its effect on the base-bulk recombination can be considered to be a second-order effect. On the other hand, the

Table 3. Impurity electrical activity and impurity limit calculated for each impurity. Also shown are the effective segregation coefficients and minority-carrier capture cross sections used in the calculation of the electrical activity. Diffusivity and solubility value extrapolated to temperatures beyond the validity region.

Impurity	Diffusivity @ RT and 850 °C [18] [cm^2 s^{-1}]	Solubility @ 850 °C [18] [cm^{-3}]	Effective segregation coefficient,[19] k_{eff} [–]	Minority-carrier capture cross section, σ_n [cm^2]	Electrical activity α [%]	Impurity limit[a] – (fitting ingot used), C_L [ppm wt (ppma)]
Cr	(2×10^{-19}) (3.6×10^{-7})	(1.7×10^{12})	3.1×10^{-6}	$\sigma_{nCrB} = 4.5\times10^{-15}$[32]	5.9	8 (4.3) – Cr40
Fe	(4×10^{-15}) 1.2×10^{-6}	(1.2×10^{13})	1.5×10^{-5}	$\sigma_{nFe} = 4\times10^{-14}$[28]	0.11	11 (5.5) – Fe50
Ti	(3×10^{-36}) 7.6×10^{-11}	$(1–7\times10^{10})$	3.5×10^{-5}	$\sigma_{nTidd} = 1.5\times10^{-15}$[29]	93	0.11 (0.065) – Ti10
Ni	(2×10^{-11}) 1.6×10^{-5}	3.5×10^{16}	–	–	–	13 (6.2) – Ni40/30 (14) – Ni200
Cu	(1×10^{-9}) 8.0×10^{-5}	(1.1×10^{17})	–	–	–	8 (3.5) – Cu100

[a] Performance degradation of about $2\%_{rel}$ at 90% of the ingot height.

IQE at 400 nm decreased in both of the Ni-contaminated ingots. The reduction increased towards the top of the ingots due to impurity segregation in the liquid phase, confirming that this effect was indeed caused by the presence of nickel, and it scaled with the concentration as well.

Copper showed an increase in the base-bulk recombination towards the top of the ingot in a similar way to Fe, Cr and Ti. However an increased recombination in the emitter, especially in the top of the ingot, was also observed.

Nickel and copper are both fast-diffusing transition metals. During wafer cooling, even without the presence of phosphorus diffusion, nickel and copper become supersaturated and diffuse to the wafer surfaces where they form precipitates. On the other hand, atoms that cannot reach the surfaces form precipitates in the bulk. The reason for copper influencing the base-bulk recombination might be related to the higher solubility (see **Table 3**) of Cu with respect to Ni (about 1 order of magnitude). In addition, Cu preferentially forms metal-rich precipitates, Cu_3Si, which do not fit well in the Si lattice, as opposed to the silicon-rich precipitates of Ni ($NiSi_2$), which present a better fit. Due the misfit of the copper precipitates, more silicon self-interstitials are emitted; therefore, copper precipitates are decorated with an extended extrinsic dislocation network,[18] potentially resulting in higher bulk recombination.

4.3. Impact on the Solar-Cell Fill Factor

The recombination in the base as well as in the emitter reasonably explains the degradation of the contaminated ingots; however, the large effect in the bottom and in the very top is not yet completely accounted for. The fill-factor (FF) decrease is another mechanism that plays a role in the (further) decrease of the solar-cell performance. As shown in **Figure 4**, the FFs of the solar cell were significantly reduced in the bottom and in the very top of the ingots contaminated at high and medium concentrations. These solar cells were mainly affected by the presence of shunts. The FF limitation, due to the link with the V_{oc} as reported by Green[20] and the minority-carrier injection-level dependency as calculated by Macdonald et al.[21] played a second-order effect here.

In the case of chromium, there was hardly any distinction in the FF degradation in the top, between the two ingots with 40 and 200 ppm wt. Iron also showed almost no difference between 50 and 200 ppm wt concentrations in the top. In Cr 4, the FF was similar to the reference, uncontaminated ingot, along the overall ingot.

In the case of nickel, the reduction in the top of the ingot with 40 ppm wt was very limited in comparison to the ingot with a similar amount of Cr. In this case, we had to consider that the atomic concentration in the melt for nickel was about 20% less than chromium (due both to the different concentrations and the different atomic weights).

An exception was for the ingot with Ni 200, for which the FF had a deeper impact from the top in comparison to the ingots with the same amount of both Cr and Fe. It is interesting to note that copper with 100 ppm wt had a FF degradation deeper from the top, in comparison with both Cr 200 and Fe 200 similar to nickel.

The impact of 10 ppm wt of Ti was much smaller towards the top, in comparison with 40 ppm wt of Fe and Cr, despite the larger degradation observed in the efficiency.

The FF degradation in the bottom of the ingots was not visible in ingots containing less than about 10 ppm wt (e.g., of

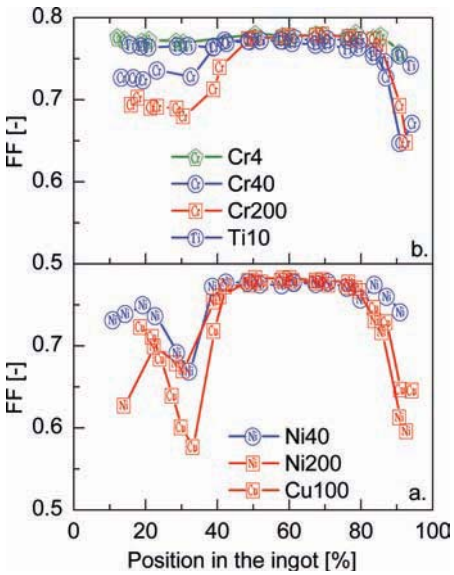

Figure 4. Fill factor versus position in the ingot. The top ingots were contaminated with chromium, iron and titanium. The bottom ingots were contaminated with nickel and copper.

chromium and titanium). Instead, above 40 ppm wt, the degradation was visible and scaled with the impurity concentration differently to that which was observed in the top. The onset for the degradation in the bottom should be in the range 10–40 ppm wt.

In conclusion the onset for the FF degradation was, to a first approximation, dependent on the amount of impurities introduced, rather than on their species. For both Cr and Fe, a similar FF degradation trend was visible at both medium (40–50 ppm wt) and high (200 ppm wt) concentrations, indicating that a kind of saturation to the FF reduction was reached.

The exception was for nickel, where the degradation at 200 ppm wt started at a lower height than for Cr and Fe at the same concentrations. The different behavior of Ni, and to some extent Cu, can be explained by its fast diffusivity in silicon, which is also responsible for the reduced IQE at short wavelength. As fast diffusers, they could easily out-diffuse during cooling, forming precipitates at the wafer surfaces. The presence of such precipitates in the emitter region can cause additional shunts that can be responsible for the greater FF reduction that is observed at high concentration (i.e., Ni 200 and Cu 100). On the contrary, at lower concentration (Ni 40), the FF degradation might be related to the same mechanism affecting the Cr and Fe (see next paragraph) since the smaller size of such precipitates did not cause the additional shunts observed in Ni 200.

In order to outline the mechanism that affects the FF degradation, images of these solar cells were taken using lock-in thermography.[22] The shunts revealed by this technique were mainly located along the grain boundaries (GBs). The shunt areas were analyzed on neighboring wafers by means of scanning electron microscopy and energy-dispersive X-ray spectroscopy. In the shunt location, we found the presence of filaments and sheets coming out from the GBs and containing nitrogen. The relation between SiN and SiC inclusions with the shunt is well documented in the literature.[23] Here it is important to note that, despite the large concentration of impurities, the cause of the severe shunt was directly related to the presence of nitrogen rather than to the impurity itself. The impurity might have nucleated the formation of such a filament or rod.[24] This can explain why the shunts were visible in the ingots with high and medium concentrations of impurities.

The appearance of this phenomenon in the bottom of the ingot might be aggravated by the geometry of the small, lab-scale furnace that was used to cast the ingots and by the use of crucibles with a spherical bottom. Circular areas in the diffusion-length maps[15] with increased crystal defects, which are centered on the original ingot centre, point in this direction.

The cause of these shunts is not well understood and the interpretation of these issues will need a dedicated study and, most likely, an adaptation of the crystallization process.

In the next section we describe a model based on the segregation of impurities to verify that this is the leading mechanism that explains the degradation trend observed at the top of the ingots.

5. Modelling

The impurity-impact model described in this section was derived to understand the main physical phenomena that contribute to the solar-cell-performance degradation along the ingot. In addition, the model provides a means of predicting the behavior of solar cells manufactured from silicon, containing known concentrations of impurities. The aim was also to define a unique parameter to quantify the 'dangerousness' of each impurity. In the first part, we based the model on degradation due to the reduction in the base-bulk lifetime of iron, chromium and titanium, while in the second part, the emitter-bulk recombination is taken into account to model the behavior of nickel. In the third part, the combination of the two effects is considered to model copper. The Scheil distribution of impurities along the ingot is the common mechanism considered in all of the models.

5.1. Base-Bulk Recombination

The assumptions for the formulation of the model are listed below:

i) The impurity distribution along the ingot height scales according to the Scheil equation $C_s = k_{eff} C_0 (1 - x)^{(k_{eff}-1)}$, where C_s is the total concentration in the solid, C_0 is the starting concentration in molten silicon, k_{eff} is the effective segregation coefficient and x is the position from the bottom of the ingot.

ii) The concentration of electrically active impurities (N_t) is proportional to the total concentration of impurities (C_s),

$$N_t = \alpha C_s \tag{1}$$

iii) The minority-carrier lifetime in the base-bulk can be described by:

$$\frac{1}{\tau_b} = \frac{1}{\tau_{imp}} + \frac{1}{\tau_{other}} = v_{th}\, \sigma_n\, N_t + \frac{1}{\tau_{other}} \tag{2}$$

where $1/\tau_{imp}$ is the recombination due to the element intentionally added, which is proportional to the concentration N_t of electrically active impurities at low injection level, and $1/\tau_{other}$ is the recombination due to other defects (i.e., not caused by the intentionally added impurity). v_{th} is the thermal velocity of the charge carrier; σ_n is the capture cross section of electrons for the respective metal.

iv) The effect of impurities on the solar cell is that of increasing the recombination in the base bulk. The solar-cell performance as a function of the base-bulk lifetime has been modelled using PC1D,[6] a software dedicated to the numerical solution of the transport equations.

Assumption (1) has been verified by neutron-activation analysis, as reported in ref.[25] The electrical activity is influenced by phenomena like precipitation, gettering and hydrogenation. Therefore the proportionality constant (α) is element dependent and is a global parameter since it correlates the electrical activity at the end of the solar-cell process with the total, initial solid-impurity concentration. In Equation (2), we discriminate between recombination due to the addition of the target impurity and recombination via defects already present in the material (e.g., unintentional contamination, grain boundaries, dislocations etc.). We used the reference ingots (not intentionally

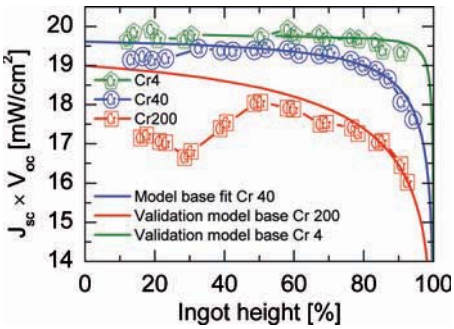

Figure 5. The product of short-circuit current and open-circuit voltage versus position in the ingot from the bottom, for the ingots contaminated with chromium. The model used is based on the degradation of the base-bulk recombination. The parameter fitting was carried out on the ingot with 40 ppm wt of chromium, obtaining an excellent fitting. The model has been validated using the ingots with 4 ppm wt and 200 ppm wt.

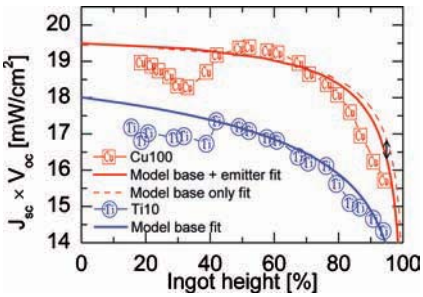

Figure 7. The product of short-circuit current and open-circuit voltage versus position in the ingot from the bottom, for the ingots contaminated with titanium and copper, separately. Titanium: the model used for titanium was based on the degradation of the base-bulk recombination. An excellent data fitting has been obtained. Copper: the model using only the base recombination overestimated the performance in the top (dash line) for copper. A better model is based on the degradation of the emitter-bulk recombination and the base-bulk recombination together. A relatively good data fitting has been obtained (solid line).

contaminated) as an estimate for $1/\tau_{other}$. We assume here that the impact of the added impurity results in recombination that is proportional to the concentration of the added impurity. In the case where the dissolved impurity dominates the recombination (i.e., negligible impact of extended crystallographic defects and precipitates), σ_n is the minority-carrier capture cross section of the point defect. Otherwise, this parameter represents an 'effective' minority-carrier capture cross section of the dominant extended defect (e.g., precipitates, etc.).

The impact of impurities on the FF cannot be modelled with a one-dimensional model since the FF is mainly limited by shunts that have a spatial distribution and involve interactions with other elements (e.g., nitrogen). Therefore we chose to model the $J_{sc} \times V_{oc}$ product of the solar cell along the ingot. The only fitting parameter of the model is the product $k_{eff} \times \sigma_n \times \alpha$.[26] C_0 is the concentration of added impurity in the feedstock. In **Figure 5**, **Figure 6**, and **Figure 7**, the fit of the model with the raw data is shown for the Cr 40, Fe 50 and Ti 10 ingots. The model fits the experimental data trend very well along the ingot height. An exception is in the bottom of the Fe 50 ingot, since degradation in the bottom is not taken into consideration in the model.

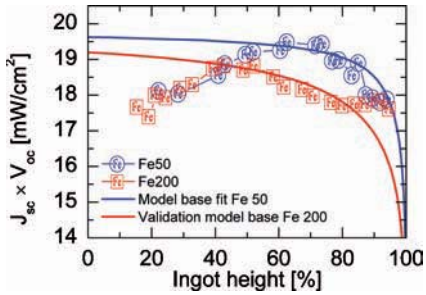

Figure 6. The product of short-circuit current and open-circuit voltage versus position in the ingot from the bottom, for the ingots contaminated with iron. The model used is based on the degradation of the base-bulk recombination. The parameter fitting has been carried out on the ingot with 50 ppm wt of iron obtaining an excellent fitting. The model has been validated using the ingot with 200 ppm wt, obtaining a good fitting of the data up to 85% of the ingot height.

The distribution of impurities according to the Scheil equation is the dominant mechanism explaining the solar-cell degradation trend along the ingot. The peculiarity of this finding is that the Scheil distribution leaves its fingerprint from the crystallization until the final solar cell. The effect of phosphorous gettering and hydrogenation reduces the impact of impurities, but the underlying trend from the Scheil equation remains. It is expected that gettering flattens the distribution of impurities along the ingot. However, a reduced gettering effectiveness has been reported towards the top of the ingots in the case of Fe, and this has been explained by the degeneration of the crystallographic structure (e.g., GBs and highly dislocated areas) as reported in ref.[15] Indeed the gettering effectiveness is known to be influenced by the presence of dislocations.[27]

In order to validate the model, the same fitting parameter for Cr 40 was used to fit the data for the ingots with 200 ppm wt and 4 ppm wt of chromium by changing only the added Cr concentration (C_0). The model predictions, both for 200 ppm wt and 4 ppm wt, overlay perfectly the experimental data (see Figure 5). An exception occurs in the bottom of the Cr 200 ingot, since the degradation there is not taken into consideration by the model. Since the effect in the bottom is visible only for higher concentrations of impurities, the model gives a good prediction for medium to low concentration levels along the entire ingot length. A similar validation has been attempted for the ingot with 200 ppm wt of Fe. It is visible in Figure 6 that the model overlaps the experimental data in the range 40 to 85% of the ingot height. A deviation is observed above about 85% where the model overestimates the impact of Fe on the solar-cell performance. To understand this deviation, we have to consider that this validation method assumes that the electrical activity α of the impurity is constant, independent from the concentration of impurities. In the case of the Fe 200 ingot, an electrical activity of 4% has been found[25] on as-grown wafers from the ratio between the interstitial and the total Fe, in comparison to an electrical activity of 10% found for Fe 50.[15] This factor-two difference in the electrical activity, even on as-grown

material, could explain the deviation in the top of the ingot. A thorough fitting of the data of the Fe 200 ingot cannot be achieved due to the relatively flat profile of the $J_{sc} \times V_{oc}$ product along the ingot.

In the model shown, the simulation of the J_{sc} and the V_{oc} separately have a maximum discrepancy of about 1% or less.

It is relevant to compare the value of α for each impurity since it reveals information about the ability of the ingot-growth and solar-cell processes to reduce the detrimental effect of the impurities by means of, for example, precipitation, gettering and hydrogenation. This parameter is not directly a fitting parameter since the product $k_{eff} \times \sigma_n \times \alpha$ is actually fitted. The effective segregation coefficient, k_{eff}, has been measured by means of Neutron Activation Analysis (NAA).[19,25] It is possible to then estimate α by assuming that the dissolved impurity dominates the recombination, and therefore σ_n is the minority-carrier capture cross section of the point defect. This assumption is not completely fulfilled since at higher concentration levels (e.g., in the top, or for ingots with high added-impurity level) the impurity interacts with the crystallographic structure increasing crystallographic defects[15,25] (e.g., GBs and dislocations) and therefore participating in and increasing the bulk recombination. However, to the extent of its validity (e.g., at lower concentrations), the estimation of α can give an indication of the impurity electrical activity. In Table 3, the values of σ_n[28–30] used to calculate α are reported. It is evident that α is as low as 0.1% for Fe. This means that just a small amount of this impurity is active or contributes to the recombination. In the case of Cr, α is about 6%, which is reasonable considering that the diffusivity is 3 times smaller and the solubility is 1 order of magnitude smaller, in comparison to iron. In the case of titanium, we assume that the dominant recombination occurs through the double-donor defect energy-level as proposed by Paudyal et al.[29] This is reasonable due to the similarity between the samples investigated there and in this study (e.g., multicrystalline ingot prepared by intentional addition of Ti in the silicon melt). Using the electron-capture cross section measured by Paudyal, α is as large as 90%. Indeed, Ti, being a slow diffuser in silicon, presents hardly any getterability and precipitation. Therefore, its electrical activity is expected to be close to the total atomic concentration.

We stress that the α values have been determined for a state-of-the-art industrial-type process, as described in Section 3. We demonstrate that these values of α can be actually achieved with the technology available today, and represent a benchmark. Therefore, best-practice industrial production should experience similar sensitivity towards the impact of impurities. In addition, these values of α are an underestimation of what can be tolerated with future developments, since no dedicated optimization (e.g., annealing, gettering, defect passivation etc.) was carried out for the intentionally contaminated ingots. A similar argument applies to the accepted impurity level C_L described in Section 6.

5.2. Emitter-Bulk Recombination

The addition of nickel to the feedstock did not reduce the base-bulk diffusion length at the solar-cell level, as reported in the previous section. Instead, nickel has the peculiar effect of reducing the IQE at short wavelengths, which corresponds to recombination taking place in the emitter region. This recombination (also often characterized as an emitter saturation current density, J_{oe}) is the combination of the emitter-bulk recombination and the surface recombination-velocity. In order to model the impact of nickel, a model for recombination in the emitter has been produced. We model the solar cell as a base and emitter volume, characterized by their bulk recombination, τ_b and τ_{be}, respectively. The bulk-base recombination is kept constant. The front-surface recombination-velocity is assumed to be constant as well, for simplicity, and further arguments for the validity of this assumption are presented below. We aimed to verify whether the bulk-emitter recombination can explain the trend of the $J_{sc} \times V_{oc}$ product along the ingot. The model used was similar to that described for base-bulk recombination, but Equation (2) now refers to the emitter-bulk recombination (τ_{be} in place of τ_b, and σ_p in place of σ_n). We have to consider that, similar to the case of base-bulk recombination, α is a global parameter that represents the fraction of impurities that contributes to recombination in the emitter, and includes phenomena like precipitation, gettering and hydrogenation. In addition, since most of the nickel in the base diffuses towards the wafer surfaces, the nickel concentration in the emitter is much higher than in the bulk, therefore α can be larger than unity and cannot be directly compared to the α estimated in the case of base-bulk recombination. We should note that N_t, σ_p and α refer to the dominant defect that is active in the n-type emitter. Since nickel precipitates quantitatively, this defect is quite likely to be nickel precipitates. Indeed Trushin et al.[31] estimated a large hole-capture cross section ($\sigma_p = 1 \times 10^{-11}$ cm^2) for $NiSi_2$. However, since both the precipitates characteristics (e.g., size and density) and the recombination parameters of Ni are not definitely known, the electrical activity α of nickel cannot be directly determined. Nevertheless, this does not prevent an attempt to fit the data to at least verify the overall validity of the model.

To this end, the $J_{sc} \times V_{oc}$ product of the solar cell along the ingot was fitted with the model. The only fitting parameter of the model is the product $k_{eff} \times \sigma_p \times \alpha$ (σ_p being the minority-carrier capture cross section of the dominant defect). In **Figure 8**, the fit of the model to the raw data is shown for the ingot with 40 ppm wt of nickel. The model fits the experimental data along the ingot height very well. This clearly demonstrates that the distribution of impurities according to Scheil is the dominant mechanism, explaining the solar-cell degradation trend along the ingot, even in the case of emitter recombination.

In order to verify that, indeed, emitter-bulk recombination explains the degradation of the solar-cell performance, we simulated J_{sc} and V_{oc} separately, using the same fitting parameters used to fit the $J_{sc} \times V_{oc}$ product. The V_{oc} is mainly degraded in comparison with the J_{sc}. We verified that the model predicts the behavior of these two parameters separately very well, and that V_{oc} is mainly responsible for the degradation.

In analogy to the procedure used above for the base-bulk recombination caused by Cr and Fe, we attempted to validate the model by using the fitting parameter from the Ni 40 ingot to then fit the data from the ingot with Ni 200, by changing only the added Ni concentration (C_0). The model strongly underestimates the $J_{sc} \times V_{oc}$ product of the Ni 200 ingot along

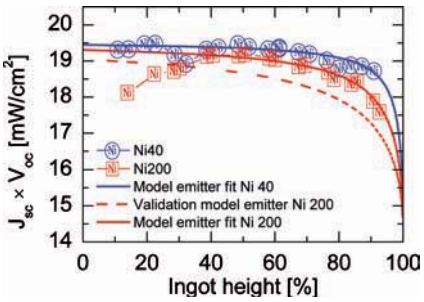

Figure 8. The product of short-circuit current and open-circuit voltage versus position in the ingot from the bottom, for the ingots contaminated with nickel. The model used was based on the degradation of the emitter-bulk recombination. The data fitting was carried out on the ingot with 40 ppm wt of nickel, obtaining an excellent fit. The model was validated using the ingot with 200 ppm wt, obtaining bad data fitting (dash line). On fitting the ingot with 200 ppm wt separately, a reduced electrical activity is found (solid line).

the ingot height. In order to fit the experimental data, the $\sigma_p \times \alpha$[32] product must be reduced by about a factor of two to obtain a good fitting. This means that the model explains the degradation trend, but either the dominant defect (σ_p) or the electrical activity (α) changes. The precipitation of nickel is not diffusion limited; therefore, one could expect that the Ni precipitates grow in size, reducing the electrical activity per Ni atom.

The simulations of the J_{sc} and the V_{oc} separately for Ni 200 (using the reduced electrical activity) have a discrepancy of about 1%. Indeed, experimentally, the Ni 200 ingot has similar V_{oc} to that of the Ni 40 ingot up to 80% of the ingot height, while the J_{sc} degrades along the overall ingot. In the $J_{sc} \times V_{oc}$ product, these two effects compensate each other, explaining the good fitting obtained.

In the device, the presence of nickel in the emitter region might have an impact on the front-surface recombination-velocity as well as on the emitter-bulk recombination. However, the model includes recombination on the base emitter alone. Building a model that includes both phenomena will unnecessarily complicate it without adding much information. Indeed, very little is known about the minority-carrier capture cross section of substitutional nickel in the bulk (interstitial nickel is unstable because it out-diffuses to the surfaces) and even less is known about the surface-recombination parameters. In addition, nickel precipitates massively and therefore recombination parameters for the precipitates need to be taken into account as well.

The diffusivity of nickel explains the different behavior of Ni in comparison to, for example, Fe and Cr. Getterable impurities like Fe or Cr should also increase recombination in the emitter. The lack of this degradation for Cr and Fe is not yet understood. We can suggest that Fe has a very-small minority-carrier cross section in the n-type emitter layer (7×10^{-17} cm^2), which could explain why iron does not reduce the IQE at short wavelengths. The same argument does not apply to Cr since its capture cross section is believed to be about 2 orders of magnitude higher, as reported by Schmidt.[30] On the other hand, if precipitates dominate recombination in the emitter, the iron- and chromium-precipitate capture cross sections should also be small, by the same argument. Very little is known about the recombination parameters of precipitates; thus, this hypothesis remains unproven. It is generally accepted that the emitter recombination is a regime limited by Auger recombination and that recombination via defect levels is a second-order effect and probably one of the reasons why gettering works. The large, estimated capture cross section of $NiSi_2$ is the only evidence that precipitated Ni is extremely active and therefore the emitter goes into a Shockley–Read–Hall limited regime, which could explain the degradation observed in the emitter.

5.3. Model for Cu

The addition of copper to the feedstock causes an impact on the IQE at long wavelength as well as at short wavelength, as is reported in the previous section. In order to model the behavior of copper, the model for the base-bulk recombination is not sufficient on its own. In Figure 7, it is shown that the $J_{sc} \times V_{oc}$ product in the top of the ingot is largely overestimated. This means that another recombination mechanism is active and becomes important in the region of the ingot where the concentration of copper increases. Therefore, we include recombination in the emitter-bulk in the model, too. To model the data, the contribution of each of the two models (base-bulk recombination and emitter-bulk recombination) needs to be determined. Fitting the $J_{sc} \times V_{oc}$ product is not possible since it is influenced by both recombination channels. Therefore, we fitted separately the IQEs at 400 nm and 1000 nm with the model for emitter-bulk recombination and base-bulk recombination, respectively. The two fitting parameters, one for each type of recombination, are the products $k_{eff} \times \sigma_p \times \alpha$ and $k_{eff} \times \sigma_n \times \alpha$, as described for the two separate models. The results of the two fittings are then given as input to PC1D[6] to calculate the $J_{sc} \times V_{oc}$ product of the combined recombination. A tentative, better fitting is visible at a higher ingot height, as seen in Figure 7.

6. Accepted Impurity Level

The effect of impurities like Fe, Cr, Ti, Ni and Cu has been modelled and the fitting parameters have been estimated. We used the model to classify the dangerousness of each impurity and to estimate the impact of a certain amount of impurities in the feedstock on the solar-cell performance. We define C_L as the limiting concentration of impurities in the molten silicon charge that results in a $J_{sc} \times V_{oc}$ product with about a 2% relative degradation with respect to the reference, uncontaminated ingot, up to 90% of the ingot height. Each impurity has a characteristic value of C_L. The meaning of C_L is that each single-impurity element, when present at this level, causes the same impact on the solar-cell performance along the ingot. It therefore represents a true measure of impurity impact. The higher the C_L value, the lower is the impact on the solar-cell level.

We estimated C_L for all of the impurities that we modelled, as shown in Table 3. The result is that 8 ppm wt of Cr, 11 ppm wt of Fe, or 0.1 ppm wt of Ti are all equivalents in terms of solar cell performances. In the case of nickel, 13 ppm wt was found for the Ni 40 ingot and 30 in the case of Ni 200 ingot. This is

due to the different electrical activity at higher concentration, as reported in the model section. The former limit (13 ppm wt) should be better considered since more restrictive and since it is inferred from ingot Ni 40 which has a contamination closer to this limit than ingot Ni 200. Copper results in a C_L value of 8 ppm wt, like chromium and similar to iron. This was quite unexpected since copper is believed to have a weaker impact on the cell performance than other impurities, mainly due to its large diffusivity. However, we need to consider that the segregation coefficient of copper[2] is about two orders of magnitude higher than iron.

Only if a single element is present and other sources of contamination (e.g., crucible, Si_3N_4 coating, etc.) provide a negligible contribution, this value can roughly be approximated to the allowed concentration of impurities in the feedstock. Note that interactions between the impurities can cause a non-linear behavior that complicates the estimate in the generic case.

It is important to note that C_L is not affected by the measurements of the effective segregation coefficient, the capture cross section and the electrical activity individually, since it is their product that is the fitting parameter. Therefore C_L directly relates the added concentration of impurities to the solar-cell performance, relying on the model assumptions alone.

The advantage of the C_L value is that it includes all the different physical properties of a specific impurity (e.g., diffusivity, solubility, getterability, segregation coefficient, etc.) in one single parameter that can be easily compared. We stress that the C_L was determined by modelling a state-of-the-art industrial-type process, described in Section 3. In addition, the results represent an underestimation of what can be achieved with future development since no dedicated optimization (e.g., annealing, gettering, defect passivation etc.) was carried out for the intentionally contaminated ingots.

The importance of C_L is relevant, not just from the feedstock point of view. Impurity contaminations can come from other sources as well, for example the purity of the crucible and the Si_3N_4 coating.[33] In addition, the construction materials and the use of catalysts or reducing agents for the fabrication of the feedstock, as well as the ingot-casting equipment, represent a known source of silicon contamination. Therefore, it is a fundamental issue for the further development of photovoltaics to accurately ascertain the impact of such impurities.

7. Conclusions

The impact of impurities on solar-cell performance was investigated. The transition metals iron, chromium, nickel, titanium and copper were considered in this study. Each impurity was intentionally added to the silicon feedstock used to grow p-type, directionally solidified, multicrystalline silicon ingots. The contamination levels were chosen, targeting typical levels of such impurities in silicon ingots, while aiming for a noticeable effect on both the wafer and cell level in comparison to the uncontaminated reference material. A state-of-the-art screen-print solar-cell process was applied to wafers cut from the ingot from the bottom to the top. The obtained solar cells were characterized and compared to reference, uncontaminated solar cells to correlate the cell performance with the impurity-contamination levels. Adding 50 ppm wt of iron or 40 ppm wt of nickel or chromium to the silicon feedstock resulted in equivalent solar-cell performances, compared to the reference, in the range of 40 to 70% of the ingot height. Addition of 10 ppm wt of titanium dramatically reduced the efficiency along the entire ingot. Impurities like iron, chromium and titanium caused a reduction in the wafer diffusion length. Nickel did not have an impact on the diffusion length, even at the highest concentration used in the feedstock (200 ppm wt). On the other hand, nickel affected the emitter recombination strongly, significantly reducing the solar-cell performance. Copper had the peculiarity of impacting both the baes-bulk recombination as well as the emitter-bulk recombination.

Two models were derived to fit the degradation along the entire ingot, based on the Scheil distribution of impurities. The solar-cell performance was modelled as a function of the base-bulk recombination and emitter-bulk recombination. The models fitted the experimental data very well. The models were also successfully validated using ingots with different concentration levels of impurities. Unexpectedly, the Scheil distribution of impurities along the ingot left its fingerprint also at the end of the solar-cell process. A measure of the impurity impact was defined as the level of impurity that causes a degradation of about 2%, up to 90% of the ingot height. This directly related the added concentration of impurities to the solar-cell performance and it was not affected by the knowledge of the effective segregation coefficient, the capture cross section and the electrical activity individually, since just their product was the fitting parameter used in the model. The result was that 8 ppm wt of Cr, 11 ppm wt of Fe, 0.1 ppm wt of Ti, 13 ppm wt of Ni, or 8 ppm wt of Cu are all equivalents in terms of solar-cell performance. The advantage of this parameter is that it comprises the different impurities' physical characteristics in one single parameter that can be easily compared.

Acknowledgements

The authors would like to thank the European integrated project "CrystalClear" (SES6-CT_2003–502583) for financial support.

[1] Photovoltaic Market Survey, *Photon International* **2009**, *1*, 170.
[2] J. R. Davis, A. Rohatgi, R. H. Hopkins, P. D. Blais, P. Rai-Choudhury, J. R. McCormick, H. C. Mollenkopf, *IEEE Trans. Electron. Devices* **1980**, *27*, 677 and reference therein.
[3] C. Häûler, G. Stollwerck, W. Koch, W. Krumbe, A. Müller, D. Franke, T. Rettelbach, *Adv. Mater.* **2001**, *13*, 23.
[4] S. Dubois, O. Palais, P. J. Ribeyron, N. Enjalbert, M. Pasquinelli, S. Martinuzzi, *J. Appl. Phys.* **2007**, *102*, 083525; Macdonald, H. Mäckel, A. Cuevas, *Appl. Phys. Lett.* **2006**, *88*, 092105.
[5] http://www.ecn.nl/publications/default.aspx?au=44311, (accessed October 2010).
[6] P. A. Basore, *IEEE Trans. Electron. Devices* **1990**, *37*, 337.
[7] C. J. J. Tool, M. Koppes, M. Fleuster, B. H. M. van Straaten, A. W. Weeber, *Proc. of the 21*th *Eu PVSEC* **2006**, *1*, 1272; A. W. Weeber, R. Kinderman, P. C. de Jong, C. J. J. Tool, in *Proc. of the 21*th *Eu PVSEC*, **2006**, *1*, 605.

[8] A. A. Istratov, T. Buonassisi, R. J. McDonald, A. R. Smith, R. Schindler, J. A. Rand, J. P. Kalejs, E. R. Weber, *J. Appl. Phys.* **2003**, *94*, 6552.
[9] D. Macdonald, A. Cuevas, A. Kinomura, Y. Nakano, L. J. Geerligs, *J. Appl. Phys.*, **2005**, *97*, 033523.
[10] Made of synthetic fused silica contanining <0.5 ppm wt Fe, Data sheet, Saint-Gobain Quartz, C10.
[11] E. Olsen, E. J. Øvrelid, *Prog. Photovoltaics* **2008**, *16*, 93.
[12] T. Buonassisi, A. A. Istratov, M. A. Marcus, B. Lai, Z. Cai, S. M. Heald, E. R. Weber, *Nat. Mater.* **2005**, *4*, 676.
[13] P. Manshanden, P. C. P. Bronsveld, L. J. Geerligs, *Proc. 24*th *EU PVSEC* **2009**, *1*, 1148.
[14] S. De Iuliis, G. Galbiati, P. C. P. Bronsveld, L. J. Geerligs, G. Coletti, presented at *Workshop on Solar Grade Silicon Feedstock Specification*, Amsterdam, The Netherlands **2008.**; M. D. Pickett, T. Buonassisi, *Appl. Phys. Lett.*, **2008**, *92*, 122103; M. Rinio, A. Yodyunyong, M. Pirker, S. Keipert, P. Wang, T. Buonassisi, D. Borchert, *Proc. 23th EU PVSEC* **2008**, *1*, 1014.
[15] G. Coletti, R. Kvande, V. D. Mihailetchi, L. J. Geerligs, L. Arnberg, E. J. Øvrelid, *J. Appl. Phys.* **2008**, *104*, 104913.
[16] F. Ferrazza, *Solid State Phenom.* **1995**, *51–52*, 449.
[17] G. Coletti, P. C. P. Bronsveld, C. Knopf, C. C. Swanson, R. Kvande, L. Arnberg, H. Habenicht, W. Warta, *Proc. 24th EU PVSEC* **2009**, *1*, 1011.
[18] K. Graff, *Metal Impurities in Silicon-Device Fabrication*, vol. *24*, 2nd ed., Springer, Berlin **1999**.
[19] G. Coletti, Effective segregation coefficient from NAA measurements, unpublished results.
[20] M. A. Green, *Solar Cells*, UNSW, Kensington, NSW, **1998**, p. 96.
[21] D. Macdonald, A. Cuevas, *Prog. Photovoltaics* **2000**, *8*, 363.
[22] J. Isenberg, W. Warta, *Progr. Photovoltaics* **2004**, *12*, 339.
[23] K. Søiland, E. J. Øvrelidb, T. A. Engha, O. Lohnea, J. K. Tuseta, Ø. Gjerstadc, *Mater. Sci. Semicond. Process.* **2004**, *7*, 39; J. Bauer, O. Breitenstein, J. P. Rakotoniaina, *Phys. Status Solidi A* **2007**, *204*, 2190; T. Buonassisi, O. F. Vyvenko, A. A. Istratov, E. R. Weber, G. Hahn, D. Sontag, J. P. Rakotoniaina, O. Breitenstein, J. Isenberg, R. Schindler, *J. Appl. Phys.*, **2004**, *95*, 1556.
[24] J. P. Rakotoniaina, O. Breitenstein, M. Werner, M. Hejjo Al-Rifai, T. Buonassisi, M. D. Pickett, M. Ghosh, A. Müller, N. Le Quang, *Proc. 20th EU PVSEC* **2005**, *1*, 773; and reference therein.
[25] G. Coletti, P. C. P. Bronsveld, R. Kvande, L. J. Geerligs, C. C. Swanson, presented at *Workshop on Solar Grade Silicon Feedstock Specification*, Amsterdam, The Netherlands **2008**.
[26] since k_{eff} is much smaller than one for most of transition metals.
[27] B. Sopori, *J. Electron. Mater.* **2002**, *31*, 972; O. Schultz, S. W. Glunz, S. Riepe, G. P. Willeke, *Prog. Photovoltaics* **2006**, *14*, 711.
[28] A. A. Istratov, H. Hieslmair, E. R. Weber, *Appl. Phys. A: Mater. Sci. Process.* **1999**, *69*, 13.
[29] B. B. Paudyal, K. R. McIntosh, D. H. Macdonald, *J. Appl. Phys.* **2009**, *105*, 124510.
[31] M. V. Trushin, O. F. Vyvenko, M. Seibt, *Solid State Phenom.* **2008**, *131–133*, 155.
[30] J. Schmidt, R. Krain, K. Bothe, G. Pensl, S. Beljakowa, *J. Appl. Phys.* **2007**, *102*, 123701.
[32] The effective segregation coefficient keff has been measured by means of NAA, see ref [25].
[33] T. Buonassisi, A. A. Istratov, M. D. Pickett, J. P. Rakotoniaina, O. Breitenstein, M. A. Marcus, S. M. Heald, E. R. Weber, *J. Cryst. Growth* **2005**, *287*, 402; R. Kvande, L. Arnberg, C. Martin, G. Rancoule, L. Dupuy, A. Holt, *Proc. 21st EU PVSEC* **2006**, *1*, 1052; B. Geyer, G. Schwichtenberg, A. Muller, *Proc. 31st IEEE PVSC* **2005**, *1*, 1059.